**Solid Freeform Fabrication 2018: Proceedings of the 29th Annual International Solid Freeform Fabrication Symposium – An Additive Manufacturing Conference**
**Reviewed Paper**

# Laser Metal Additive Manufacturing on Graphite

Arad Azizi[1], Scott N. Schiffres[1,2*]

[1] Department of Mechanical Engineering, Binghamton University, Binghamton, NY 13902.
[2] Department of Materials Science & Engineering, Binghamton University, Binghamton, NY 13902.
* Corresponding author sschiffr@binghamton.edu

## Abstract

Metal powders are typically directly fused to a metal substrate of similar composition in metal powder-bed fusion additive manufacturing. This work presents a process for printing a metal alloy directly on graphite, rather than a metal platform. This technology has attractive applications to heat transfer, as this process can be used to directly print heat sinks or heat exchangers on pyrolytic graphite. The heat transfer applications of metal-pyrolytic graphite are enormous, as pyrolytic graphite has the second highest thermal conductivity (>1700 W/m-K at room temperature) of any bulk material, with only expensive diamond exceeding it. Bonding of common metal alloys used in additive manufacturing and graphite are relatively weak and possess high contact angles. However, by using the proper interlayer material, wettability and reactivity of the graphite substrate with metal powder can increase drastically. The alloys that can typically bond to graphite require extended times at elevated temperatures (minutes to hours), while this study demonstrates rapid bonding (~100 µs).

*Keywords*
Dissimilar material bonding; Powder bed fusion; Selective laser melting (SLM); Laser material processing; Graphite-Metal bonding

## Introduction

The graphite crystal structure consists of strong graphene planes ($sp^2$ bonded carbon) which are connected by weaker interplanar Van der Waals forces [1,2]. The thermal conductivity in the graphene plane is extraordinary (>1700 W/m-K) over eight times better than aluminum. The thermal conductivity of pyrolytic graphite makes it an attractive material for use as a heat spreader, especially when coupled with a heat pipe or heat exchanger that is additively printed. Furthermore, graphite is 16% lighter than aluminum. Graphite also possesses beneficial properties for nuclear applications.

One of the key challenges in metal additive manufacturing is the removal of the printed part from build platform. Conventional platforms are made of the same material as the metal powder to achieve reliable bonding and resistance to thermal stress. Support or solid structures are used to provide the required offset for the cutting blade to detach the part from build platform followed by detailed machining to achieve proper surface finish. This process adds additional machining, particularly challenging to machine metals, like titanium or stainless steel. Another benefit is that

current building platforms used in commercial metal printing devices are heavy. These blocks need to be removed each time the process completes. Since graphite is lightweight, it can help to make handling and post-machining easier and safer.

Studying wetting of metal alloys on substrates of dissimilar material can provide valuable insights regarding bonding. However, there are debates regarding the mechanism of wetting in metal alloy systems at high temperatures. In non-reactive systems, it is hypothesized that wetting occurs by displacement of molecules of advancing front on adsorption sites of the substrate originated from surface tension. Interdiffusion and dissolution of the substrate directly affects the composition of the liquid and as a result solid-liquid interfacial energy [3]. For reactive systems, wetting is limited by the diffusion of reactive elements and local reaction kinetics [4].

The joining of dissimilar materials such as graphite to common metals employed in additive manufacturing is challenging due to these metals having contact angles greater than 130° (*i.e.*, non-wetting) [1]. Reactive metals like Ti, Ta, Zr and Nb have been bonded to graphite by forming metal-carbide interlayers. This process is done by holding the sample in a furnace at around 1000 °C for 90 minutes [5]. The wetting behavior is the result of carbide formation at the interface by diffusive transport of reactive species, which minimizes the surface energy of the system [1]. The bonding time for these conventional bonding techniques is very long (minutes to hours), compared to laser exposure period of a single voxel in additive manufacturing (~100 µs).

Previously, rods of Graphite and SUS304 stainless steel were joined by solid state diffusion bonding under a compressive pressure of 25 MPa and a temperature of 664 °C in 120 minutes. Clearly, this methodology is not applicable to additively bonding metal powder to graphite as the basic requirements of bonding time and pressure cannot be satisfied [6]. In another study carbon-carbon composites were brazed to stainless steel 316L at a temperature of 1050 °C using BNi-7 (Ni-14Cr-10.5P-0.1Si) filler alloy. Observation of the microstructure confirmed the formation of carbides. Joint shear strength of approximately 16 MPa were reported for a 1mm thick Nb interlayer [7]. Sn-Ti-Ag alloys are considered “active” alloys that bond to various materials including many metals, ceramics, and carbon materials at temperatures between 250 °C to 450 °C. [8] Based on a thermodynamics study on Sn-Ti-Ag filler alloys, the activity of Ti increases with weight percentage between 0 and 2.25 wt % at 450 °C. The addition of silver at low mass fractions (less than 10 wt%) tends to increase the titanium activity at 450 °C but increasing silver concentration beyond that point has diminishing returns, [9] hence Ag concentrations of less than 10 wt% are desirable.

The contact angles of Sn-Ti and Ag-Ti alloys on graphite reduce to under 10° by adding approximately 2-5 wt% Ti to the systems. As a result, it is expected to see acceptable wetting on graphite. Also in the case of using the alloy as interlayer to bond steel to graphite, the reactive wetting mechanism of Sn/Fe system is due to the formation of $FeSn_2$ at the interface [10].

## Methods

All experiments were performed with Binghamton University's EOS m290 system under a $N_2$ atmosphere with $O_2$ concentrations of less than 1.5%. Superfine isomolded graphite with a grade of GM-10 was purchased from GraphiteStore.com. Stainless steel 316L metal powder was sourced from EOS [11]. Silver, titanium and tin powders with respective average diameters of 5µm, 10µm and 40 µm and purities of above 99% were mixed with a custom powder mixer.

The graphite samples were roughened by laser ablation using a laser power of 200 W and a scan rate of 1000 mm/s. This ablated about an RMS depth of 29.8 µm (measured by Veeco NT1100 optical profilometer). Three-dimensional topography of the surface at the edge of exposed area to laser scan can be seen in Figure 1. The roughened surface led to better adhesion by exposing clean graphite surface and improving wetting behavior [1]. This step could possibly be omitted, though with weaker bonding.

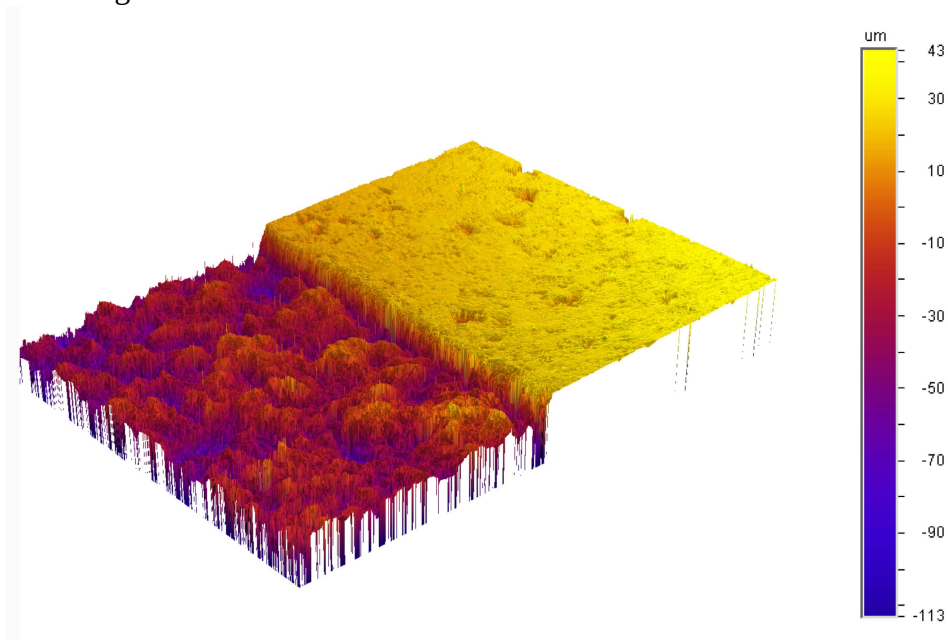


Figure 1: Optical profilometry of ablated graphite. The area scan size is 1.7 × 2.3 mm.

Phase transformation and reactive wetting are dictated by laser matter interactions, transport and reactions during this process. Various powers ranging from 30 to 200 watts and scanning rates from 800 to 6500 mm/s with constant hatch distance of 0.09 mm were tested to find the exposure parameters that provide the highest wetting and bonding strength between graphite and the alloy. During this process, it is observed that at a fixed scanning speed, low power will result in partial sintering behavior and high power causes high vapor flux and large recoil pressure which leads to splattering. These process parameter trends with scan rate and power agree with the general process parameters seen for other materials [12]. One key difference with regular stainless steel processing is that the mixed powder phase transformation is assisted by a double laser exposing each layer. The bonding appears to be a two-step process that requires a double exposure. The reason for this double exposure is an ongoing area of research.

A naïve demonstration of stainless steel 316L printing on graphite was performed as a control experiment with various exposure parameters. The results indicated poor wetting for all tests (Figure 2).

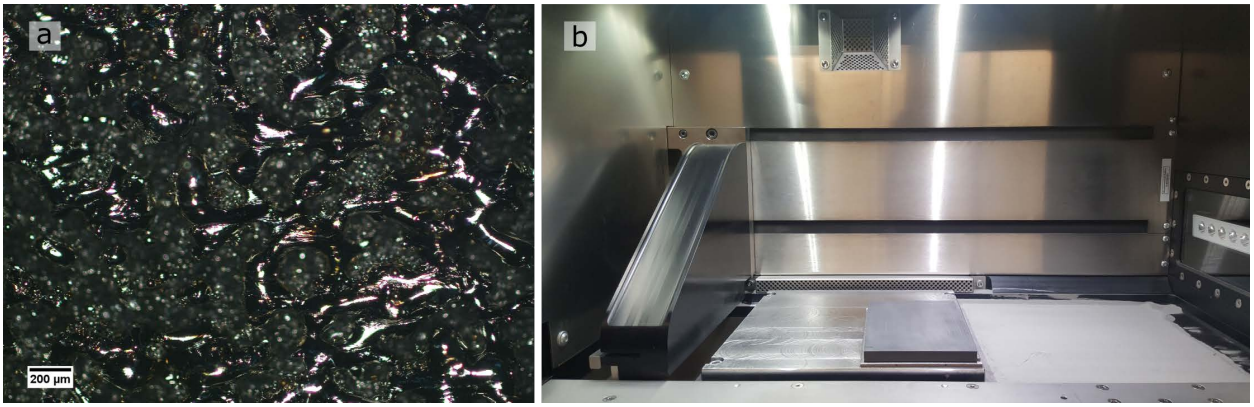


Figure 2: a) Optical image of stainless steel 316L deposited on graphite. b) Fixture designed to hold graphite substrate on build platform of EOS M290.

In an experiment, three layers of the Sn-Ag-Ti alloy with a thickness of 40 µm each are deposited onto graphite surface by laser melting. Afterwards, two layers of powder mixed with 50 wt% of stainless steel 316L deposited with same exposure parameters to create an elemental gradient. Following layers are built with SS316L material using the support structure exposure parameters. Using this process, the Binghamton University logo was printed. By heating the alloy to 400 °C, the graphite platform can be easily parted from the stainless steel logo (Figure 3).

Figure 3: a) Stainless steel logo printed on graphite. b) Removing printed part using hot plate.

## Results and discussion

Sessile drop contact angle measurements generally use molten metal drops to determine contact angles, but are not readily applied to selective laser melting as phase change occurs fast (~100 µs)

and the molten metal cannot be easily visualized in cross-section. In SLM the molten metal drop solidifies before reaching its equilibrium state [13,14]. Nonetheless, the post-solidified contact angle provides information regarding the wetting mechanism during laser processing [1]. Five lines of 120 µm width on graphite were produced to measure the contact angle versus scan rate. Each line was scanned by a different laser exposure ranging from 5000 mm/s to 6000 mm/s with a fixed laser power of 150 watts. By optical profilometry (Figure 4) the height-to-width (H/D) ratios were measured for each line and used to determine contact angle. By lowering the scan speed, the laser heating period and maximum temperature increases, which improves the diffusion of reactants, assisting spreading. Vaporization induced defects (spattering and vaporization) become more frequent at scan rates slower than 5000 mm/s

The energy barrier for diffusion and crystallization must be overcome with thermal energy, as the reaction rate and diffusivity are expected to have an Arrhenius rate dependence, $exp(-E_a/k_BT)$, where $E_a$ is the activation energy, $k_B$ is the Boltzmann constant , and $T$ is absolute temperature [15]. Due to the hot laser processing temperature, the energy barrier to atoms diffusing and crystallizing can be overcome more rapidly than reactions just above the melting point of the metal, explaining why this bonding occurs so rapidly.

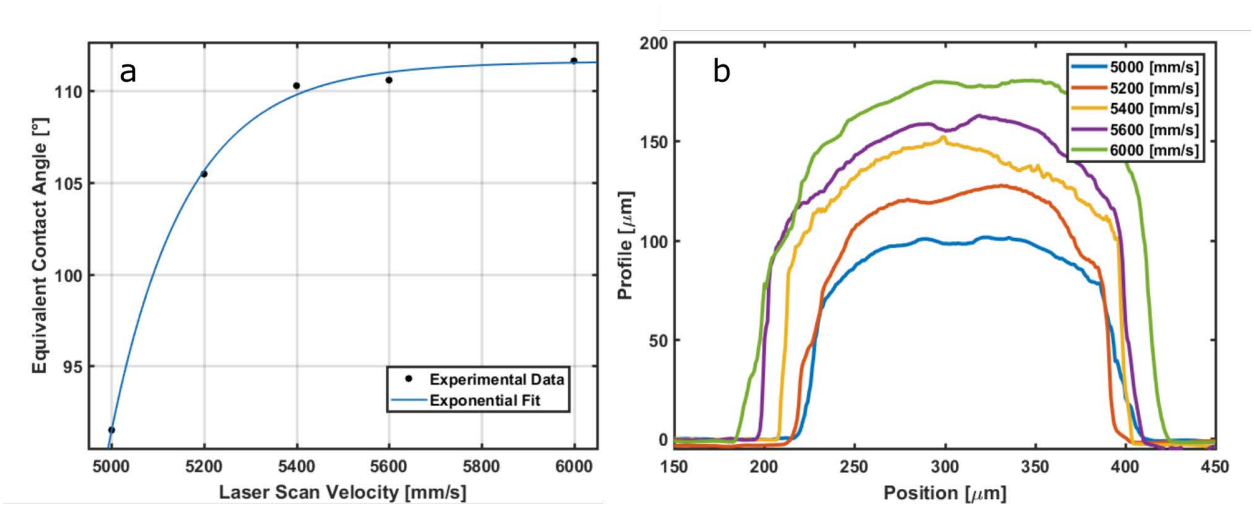


| Scan Velocity [mm/s] | Width (D) [µm] | Height (H) [µm] | H/D Ratio | θ equivalent |
|---|---|---|---|---|
| 5000 | 197.7 | 101.50 | 0.51340 | 91.51520 |
| 5200 | 194.3 | 127.65 | 0.65697 | 105.4526 |
| 5400 | 202.5 | 145.30 | 0.71753 | 110.2597 |
| 5600 | 225.7 | 162.86 | 0.72158 | 110.5620 |
| 6000 | 245.4 | 180.58 | 0.73586 | 111.6096 |

Figure 4: a) Contact angle versus laser exposure parameters, b) profilometry scans used to determine contact angle

Since the alloy-graphite bond is under combined normal and shear stresses imposed by the contraction of the metal on cooling, it is necessary to measure the bonding strength of the joint. The common approach is to perform tensile tests to calculate yield tensile strength and shear yield

strength of the joint. However, these tests are designed for isotropic or homogenous materials, which are not the case at the interface [16,17]. To characterize the joint, a lap shear test according to Figure 5 was performed, where the alloy layer functions as a weld connecting two graphite blocks that are loaded under tension.

Figure 5: Schematic of the shear lap test

The designed mechanical testing reveals the lower limit of interfacial strength for the alloy in figure 6. Since the fracture occurred in alloy for most of the samples rather than at the graphite-metal interface, only a lower limit of the interfacial strength can be estimated (shown by arrow).

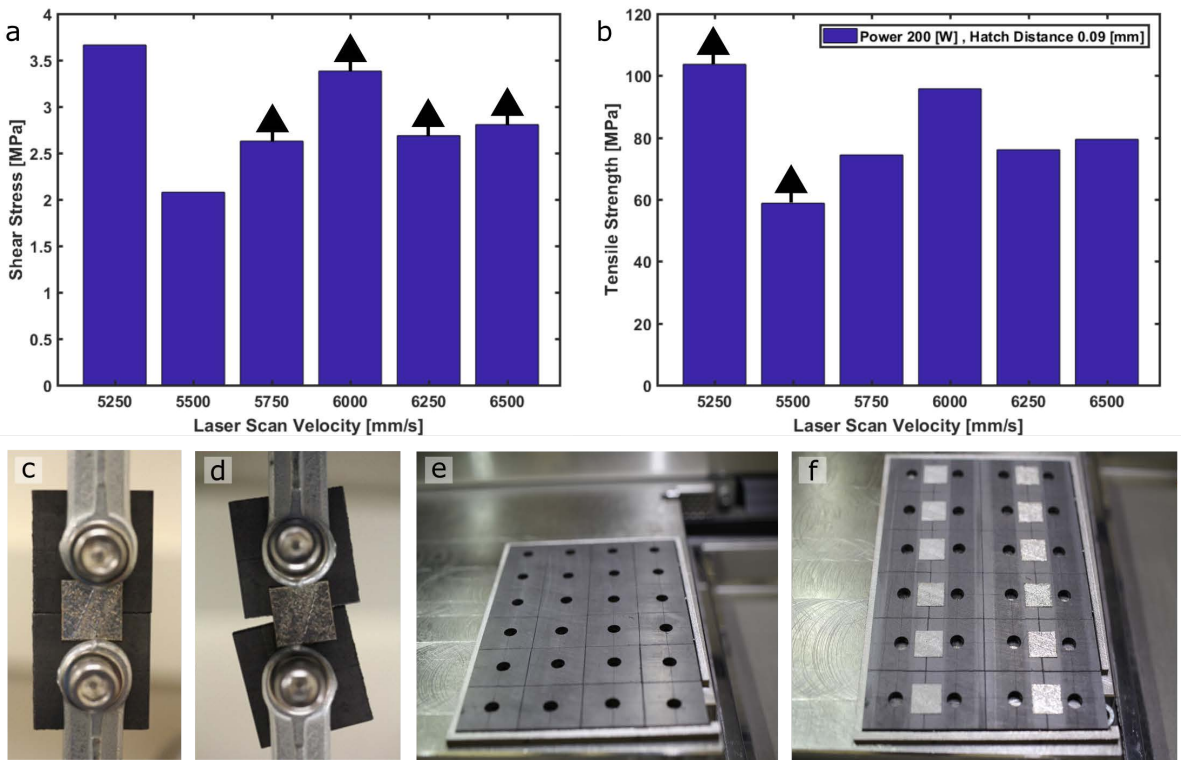

Figure 6: Interfacial strength of the graphite-metal bonding at various laser scan velocities (a, b). Sample preparation for tensile test (c, d, e, f).

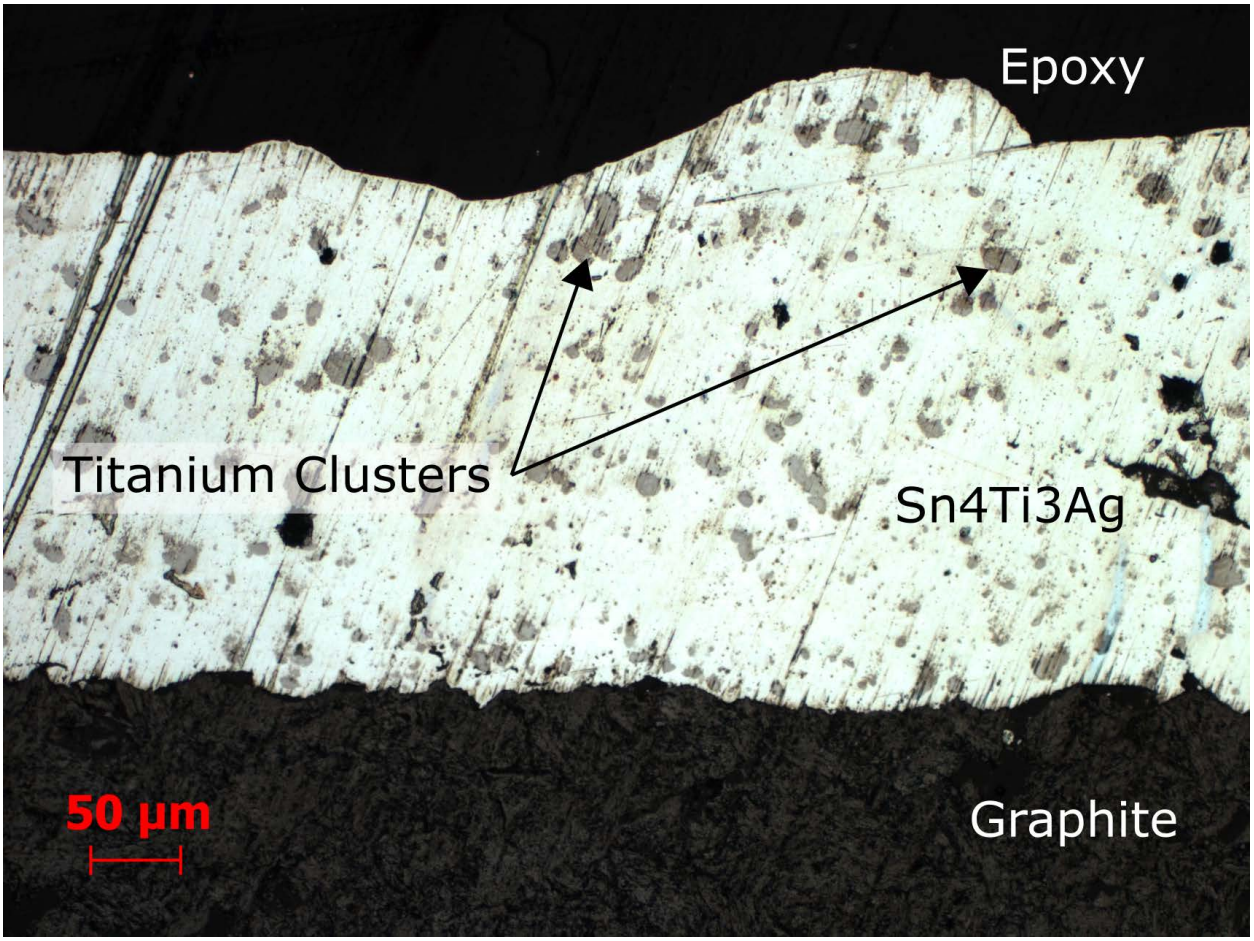

Figure 7: Optical image of the interface containing titanium-tin intermetallic phases.

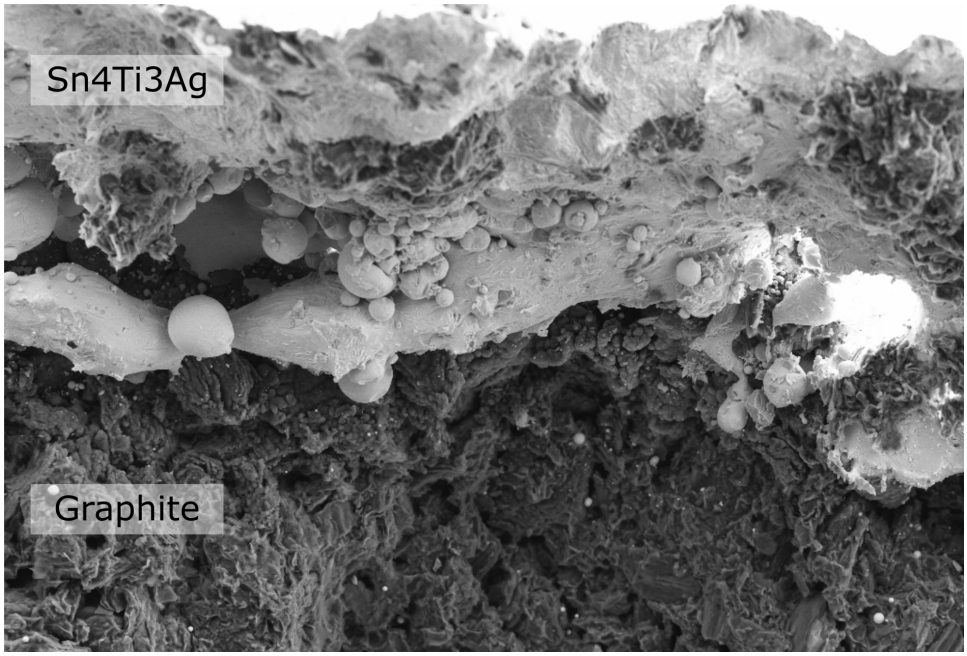

Figure 8: Unpolished scanning electron microscopy of graphite -Sn4Ti3Ag interface (EHT= 15kV, WD=9.9 mm, SE2 detector).

Energy-dispersive X-ray spectroscopy (EDS) was performed on the interface of the joint (Figure 9). A scan across the interface shows diffusion of carbon into the alloy. Elemental compositions observed at the interface show a titanium-tin-carbide [18].

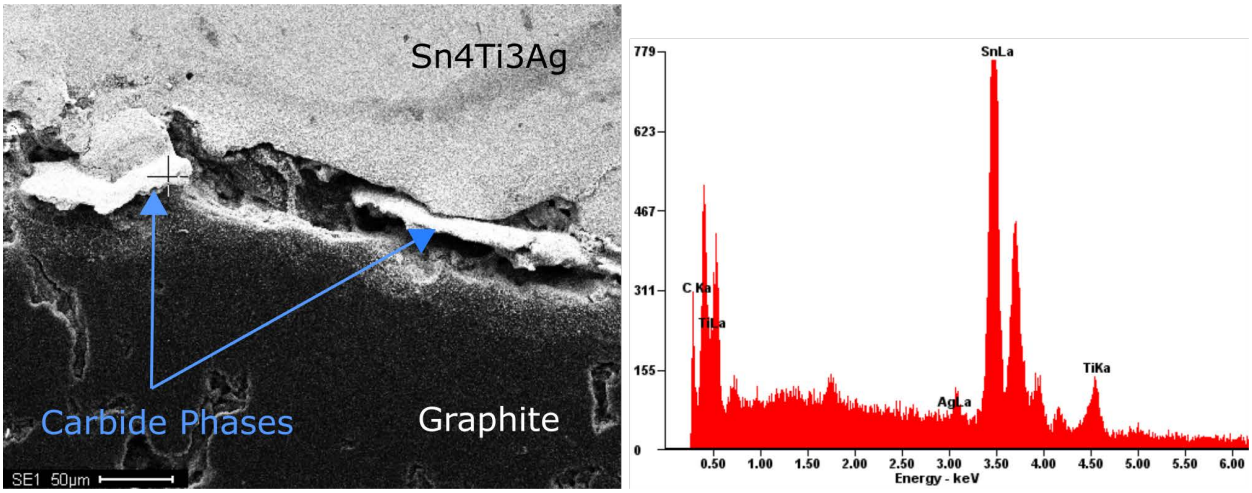


| Element | C | Ag | Sn | Ti |
|---|---|---|---|---|
| At% | 25.85 | 00.00 | 61.92 | 12.22 |
| Wt% | 03.77 | 00.00 | 89.13 | 07.10 |

Figure 9: a) SEM image of graphite-Sn4Ti3Ag interface (EHT=15 kV, WD=8.5 mm), b) Sample of EDS point scan across the interface (DT~30%)

To examine the reliability of the bond in various thermal conditions, a thermal cycling test was performed. The bulk SS316L samples printed on graphite were tested using a Thermotron SM-8 chamber (Figure 10). During the test, the chamber temperature varied from -40 °C to 130 °C for 100 cycles. The temperatures of the parts are monitored. After the 100 cycles (over 1 week of testing), the parts were visually examined for defects, such as delamination, along the perimeter where the thermal stresses are greatest. All parts passed the visual test without any noticeable failure or defects.

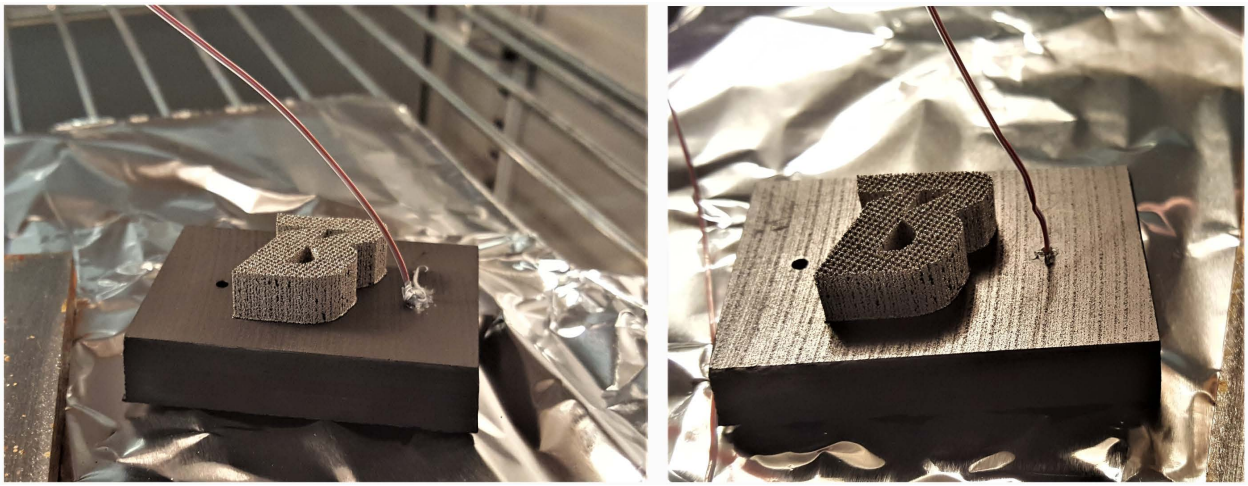

Figure 10 Two stainless steel parts after thermal cycling test

## Conclusion

We have demonstrated for the first time an additive manufacturing process capable of bonding metals onto graphite. These parts can help effectively spread heat and take advantage of the high in-plane thermal conductivity of pyrolytic graphite. Furthermore, graphite can be used as an alternative build platform which decreases the cost of printing with stainless steel or titanium since current metal additively manufactured parts require machining to remove support, which requires either manually machining the parts or computer-controlled machining (CNC), which are both expensive and time-consuming. By the proposed technology, there is no need to print support structures as the part can be printed directly on the build platform and separated from it after print by melting the alloy connecting the stainless to graphite, or by brittle fracturing the graphite plate. The interlayer alloy used in this research is a demonstration of how this process works and further studies of microstructure are warranted. While these experiments were performed on isomolded graphite, similar performance can also be achieved on pyrolytic graphite with slightly adjusted processing parameters. Building on pyrolytic graphite may be desired for certain applications that demand high thermal conductivity and excellent heat spreading, as the in-plane thermal conductivity exceeds 1,700 W/m-K [19].

## Acknowledgements

We thank Dr. Junghyun Cho for use of various sample preparation tools, Dr. Changhong Ke for the helpful mechanical testing discussions, Mr. Benson Chan and Dr. Stephen Cain at Binghamton University's Integrated Electronics Engineering Center for the thermal cycling testing, Scott Volk and Shawn Leonard of Incodema3D for their valuable advice on the EOS m290 system. S.N.S gratefully acknowledges the support of SUNY Binghamton through his startup funds and the ADL's Small Grant (ADLG173). This technology relates to the authors' patent application 62/717444.

## References

[1] Nicolas Eustathopoulus, Michael G. Nicolas, Béatrice Drevet, eds., Wettability at High Temperatures, Pergamon, 1999.

[2] H. Zabel, S. Solin, eds., Graphite Intercalation Compounds I, Springer Berlin Heidelberg, Berlin, Heidelberg, 1990. doi:10.1007/978-3-642-75270-4.
[3] E. Saiz, A.P. Tomsia, Atomic dynamics and Marangoni films during liquid-metal spreading, Nature Materials. 3 (2004) 903–909. doi:10.1038/nmat1252.
[4] N. Eustathopoulos, Progress in understanding and modeling reactive wetting of metals on ceramics, Current Opinion in Solid State and Materials Science. 9 (2005) 152–160. doi:10.1016/j.cossms.2006.04.004.
[5] M. Tashiro, A. Kasahara, Method of bonding graphite to metal, US5904287 A, 1999. http://www.google.com/patents/US5904287 (accessed November 28, 2017).
[6] H. Sueyoshi, T. Nishida, Solid State Bonding of Graphite to SUS304 Steel, Materials Transactions, JIM. 41 (2000) 414–419. doi:10.2320/matertrans1989.41.414.
[7] J.Y. Liu, S. Chen, B.A. Chin, Brazing of vanadium and carbon-carbon composites to stainless steel for fusion reactor applications, Journal of Nuclear Materials. 212–215 (1994) 1590–1593. doi:10.1016/0022-3115(94)91095-2.
[8] R.W. Smith, Process of using an active solder alloy, US6047876A, 2000.
[9] Y. Tang, G. Li, Thermodynamic Study of Sn-Ag-Ti Active Filler Metals, Physics Procedia. 25 (2012) 30–35. doi:10.1016/j.phpro.2012.03.045.
[10] Q. Lin, W. Zhong, F. Li, W. Yu, Reactive wetting of tin/steel and tin/aluminum at 350–450 °C, Journal of Alloys and Compounds. 716 (2017) 73–80. doi:10.1016/j.jallcom.2017.05.036.
[11] EOS Metal Materials for Additive Manufacturing, (n.d.). https://www.eos.info/material-m (accessed November 28, 2017).
[12] S.A. Khairallah, A.T. Anderson, A. Rubenchik, W.E. King, Laser powder-bed fusion additive manufacturing: Physics of complex melt flow and formation mechanisms of pores, spatter, and denudation zones, Acta Materialia. 108 (2016) 36–45. doi:10.1016/j.actamat.2016.02.014.
[13] T. Young, III. An essay on the cohesion of fluids, Phil. Trans. R. Soc. Lond. 95 (1805) 65–87. doi:10.1098/rstl.1805.0005.
[14] M.E. Schrader, Young-Dupre Revisited, Langmuir. 11 (1995) 3585–3589. doi:10.1021/la00009a049.
[15] R. Lacmann, Crystallization, Third Edition. J. W. MULLIN, Butterworth-Heinemann, Oxford 1997, 527 Seiten, zahlr. Abb. und ISBN 0-7506-3759-5, Chemie Ingenieur Technik - CIT. 70 (1998) 1468–1468. doi:10.1002/cite.330701126.
[16] R.M. Christensen, A Two-Property Yield, Failure (Fracture) Criterion for Homogeneous, Isotropic Materials, J. Eng. Mater. Technol. 126 (2004) 45–52. doi:10.1115/1.1631024.
[17] Y. Flom, 2 - Strength and margins of brazed joints, in: D.P. Sekulić (Ed.), Advances in Brazing, Woodhead Publishing, 2013: pp. 31–54. doi:10.1533/9780857096500.1.31.
[18] Y.C. Zhou, H.Y. Dong, B.H. Yu, Development of two-dimensional titanium tin carbide (Ti2SnC) plates based on the electronic structure investigation, Materials Research Innovations. 4 (2000) 36–41. doi:10.1007/s100190000065.
[19] G.A. Slack, Anisotropic Thermal Conductivity of Pyrolytic Graphite, Phys. Rev. 127 (1962) 694–701. doi:10.1103/PhysRev.127.694.